ORNL/TM-2021/2064

Fracture Toughness Characterization of Generation II FeCrAl Alloys after ~18 dpa Irradiation

X. Chen[1], K.G. Field[1,2], A. Campbell[1], J. Werden[1], Y. Yamamoto[1], R. Howard[1,3], C. Massey[1], K. Linton[1], A. Nelson[1]

[1]Oak Ridge National Laboratory
[2]Now at University of Michigan
[3]Now at Idaho National Laboratory

August 2021

OAK RIDGE NATIONAL LABORATORY
MANAGED BY UT-BATTELLE FOR THE US DEPARTMENT OF ENERGY

ORNL/TM-2021/2064

Advanced Fuels Campaign

FRACTURE TOUGHNESS CHARACTERIZATION OF GENERATION II FECRAL ALLOYS AFTER ~18 DPA IRRADIATION

Xiang (Frank) Chen[1], Kevin G. Field[1,2], Anne Campbell[1], Jesse Werden[1], Yukinori Yamamoto[1], Richard Howard[1,3], Caleb P. Massey[1], Kory D. Linton[1], Andrew T. Nelson[1]

[1]Oak Ridge National Laboratory
[2]Now at University of Michigan
[3]Now at Idaho National Laboratory

Date Published: August 2021

Prepared by
OAK RIDGE NATIONAL LABORATORY
Oak Ridge, TN 37831-6283
managed by
UT-BATTELLE, LLC
for the
US DEPARTMENT OF ENERGY
under contract DE-AC05-00OR22725

CONTENTS

ACKNOWLEDGEMENT

This research was sponsored by the U.S. Department of Energy, Office of Nuclear Energy, Advanced Fuels Campaign Program, under contract DE-AC05-00OR22725 with UT-Battelle, LLC. A portion of this research at High Flux Isotope Reactor of Oak Ridge National Laboratory (ORNL) was sponsored by the Scientific User Facilities Division, Office of Basic Energy Sciences, US Department of Energy.

We appreciate contributions from the following personnel at ORNL: Eric Manneschmidt for performing hot cell entries to install test equipment; Clay Morris and Mark Delph from the Irradiated Materials Examination and Testing facility in arranging and facilitating hot cell testing; Stephanie Curlin from Low Activation Materials Development and Analysis facility for dilatometer measurements of SiC thermometry specimens. Lastly, we would like to thank Lizhen Tan and TS Byun for their thoughtful review of this report before publication.

EXECUTIVE SUMMARY

FeCrAl alloys are promising candidate materials for the accident tolerant fuel (ATF) cladding applications due to their excellent corrosion resistance to the elevated temperature steam environment. Currently, the handbook on FeCrAl material properties contains only limited data regarding the fracture toughness properties of any FeCrAl alloy. This includes alloys currently under investigation within the Advanced Fuels Campaign (AFC) at Oak Ridge National Laboratory (ORNL). In this project, a series of irradiation capsules have been irradiated in the High Flux Isotope Reactor (HFIR) at ORNL with two Generation II FeCrAl candidate alloys, i.e., C06M and C36M, to assess the fracture response of these alloys after neutron irradiation. These alloys represent the "book-end" compositions for C26M, the alloy currently being developed as the leading candidate for LWR cladding. A total of six irradiation capsules were irradiated in HFIR at target temperatures of 200°C, 330°C, and 500°C up to target damage doses of 8 displacements per atom (dpa) and 16 dpa. These damage doses represent the expected middle and end of life damage levels for typical LWR cladding while the irradiation temperature regimes will provide insight into the role of varying microstructural features on the fracture toughness properties of neutron irradiated FeCrAl alloys. To date, irradiation of all capsules has been completed in HFIR. This report summarizes the latest results of microhardness and fracture toughness PIE for the 16 dpa capsules (FCAB2, FCAB4, and FCAB6), for which the measured irradiation conditions were: 204°C/17.6dpa, 343°C/18.3dpa, and 507°C/18.6dpa. The main conclusions of this study can be summarized as follows:

1) After the 204°C/17.6dpa irraidation, both C06M and C36M exhibited significant irradiation hardening and embrittlement
2) After the343°C/18.3dpa irraidation, both C06M and C36M exhibited small irradiation hardening without irradiation embrittlement
3) After the 507°C/18.6dpa irraidation, both C06M and C36M exhibited irradiation softening without irradiation embrittlement
4) Comparing the microhardness and Master Curve reference temperature T_{0q} before and after neutron irradiation, we did not observe a linear correlation between the two parameters for both C06M and C36M. This should be mainly due to a flat response of the Master Curve reference temperature T_{0q} to the irradiations at 166-204°C and 315-343°C ranges
5) C06M showed a lower T_{0q}, meaning better toughness, than C36M at the unirradiated condition and such trend was kept even after neutron irradiation except for the 166-204°C irradiation where both materials had similar T_{0q}.
6) In terms of hardening and embrittlement, the irradiation effect on both C06M and C36M appeared to saturate after an irradiation dose of 7 dpa.

1. INTRODUCTION

The handbook of FeCrAl material properties [1] contains only limited data on the fracture toughness properties of FeCrAl alloys, including Oak Ridge National Laboratory (ORNL) derived FeCrAl alloys investigated under the Advanced Fuels Campaign (AFC) program. Datasets on unirradiated materials developed both by ORNL [2] and from the literature [3] using Charpy V-notch specimens to determine the ductile to brittle transition temperature (DBTT) show key findings including (i) increasing Al and/or Cr content can raise the DBTT of FeCrAl alloys, (ii) DBTT values can typically reside at or above the room temperature for FeCrAl alloys, and (iii) grain size and residual strain can affect the fracture properties. These results suggest that the fracture toughness of FeCrAl alloys may be a critical factor in its deployment for nuclear power applications, but no studies have been completed prior regarding the DBTT or fracture toughness of FeCrAl alloys after neutron irradiation, especially for the leaner Cr content alloys currently under investigation as candidate alloys for light water reactor (LWR) cladding.

Taken in isolation, embrittlement of a cladding alloy during service has no bearing on possible licensure. Hydriding of zirconium cladding alloys is well understood to result in significant embrittlement. Furthermore, mechanical failure of irradiated cladding containing fuel pellets occurs at far higher stresses than defueled cladding samples because the presence of the fuel toughens the fuel rod. Despite this absence of direct relevance to licensure, radiation embrittlement is a fundamental structure-property evolution that should be understood to guide the further development of FeCrAl alloys. Licensure of FeCrAl incorporates far more complex system behaviors that will not be possible until larger quantities of fueled irradiated rodlets are available.

Recently, a series of irradiation capsules have been irradiated in the High Flux Isotope Reactor (HFIR) with candidate Generation II FeCrAl alloys to assess the fracture response of these alloys after neutron irradiation. The name of this irradiation program is called the FCAB (FeCrAl-Bend Bar) irradiation program. The FCAB program irradiates the M4CVN (miniature 4-notch Charpy V-notch) bend bar geometry. Four bend bar specimens with four notches for each specimen were irradiated per capsule with two different alloys included: C06M and C36M. These alloys represent the “book-end” chromium compositions (10 and 13 wt.% Cr nominal, respectively) for C26M, the alloy currently being developed as the leading candidate for LWR cladding. A total of six irradiation capsules were irradiated in HFIR at target temperatures of 200°C, 330°C, and 500°C up to target damage doses of 8 displacements per atom (dpa) and 16 dpa. These damage doses represent the expected middle and end of life damage for typical LWR cladding while the temperature regimes will provide insight into the role of varying microstructural features on the fracture toughness properties of neutron irradiated FeCrAl alloys. Additional details regarding the design of the experiment for the FCAB irradiation program can be found elsewhere [4]. To date, irradiation of all capsules has been completed in HFIR. The post-irradiation examination (PIE) results for the 8 dpa capsules (FCAB1, FCAB3, and FCAB5) can be found in an earlier report [5]. This report summarizes the latest results of microhardness and fracture toughness PIE for the 16 dpa capsules (FCAB2, FCAB4, and FCAB6).

2. EXPERIMENTAL

2.1 MATERIALS AND SPECIMENS

Two Generation II FeCrAl alloys, namely C06M and C36M, were selected to study the Cr composition dependence on irradiated FeCrAl fracture toughness. The nominal and analyzed compositions of the two materials are summarized in Table 1. Both alloys met the initial design target for their compositions.

Table 1. Nominal and analyzed compositions for C06M and C36M

Alloy		Composition, wt.%									
		Fe	Cr	Al	Y	Mo	Si	C	S	O	N
C06M	Nominal	81.77	10	6	0.03	2	0.2				
	Analyzed	81.80	10.03	6.00	0.01	1.96	0.18	0.0030	0.0012	0.0016	0.0004
C36M	Nominal	78.77	13	6	0.03	2	0.2				
	Analyzed	78.80	12.98	6.00	0.04	1.98	0.18	0.0030	<0.0003	0.0016	0.0002

A miniature four Charpy V-notch bend bar specimen, called M4CVN, was used in fracture toughness characterization. Figure 1(a) illustrates the M4CVN specimen design and Figure 1(b) shows the actual machined specimens for C06M and C36M [6]. The M4CVN specimen follows the same size ratio of the bend bar specimen design in ASTM E1921 [7]. Since the loading portions are shared between neighboring notches, the M4CVN specimen design consumes less material than the standard single notch bend bar specimen and is favorable for more efficient use of irradiation facilities and reducing the specimen dose rate after irradiation. Each notch of M4CVN specimens was fatigue pre-cracked to a nominal crack size to width ratio of ~0.5 before fracture toughness testing and neutron irradiation. The fracture toughness specimens were machined from the plate material in the assumed T-L direction, i.e., the fracture plane normal direction is perpendicular to the material rolling direction and the crack propagation direction is parallel to the material rolling direction.

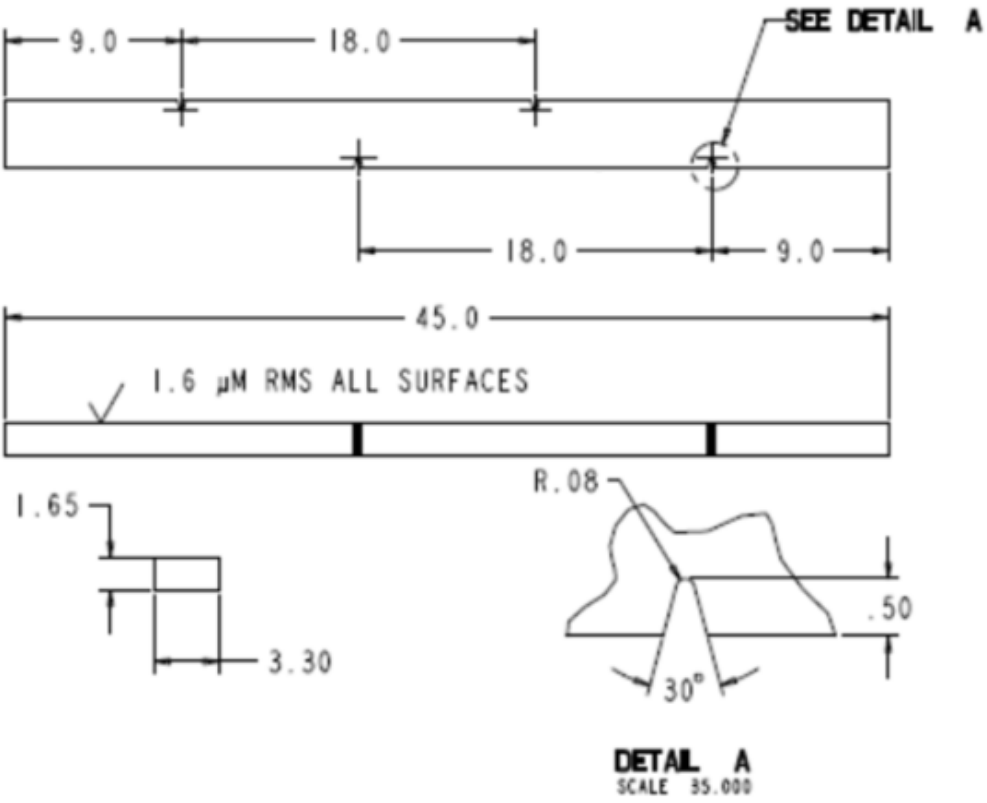

(a)

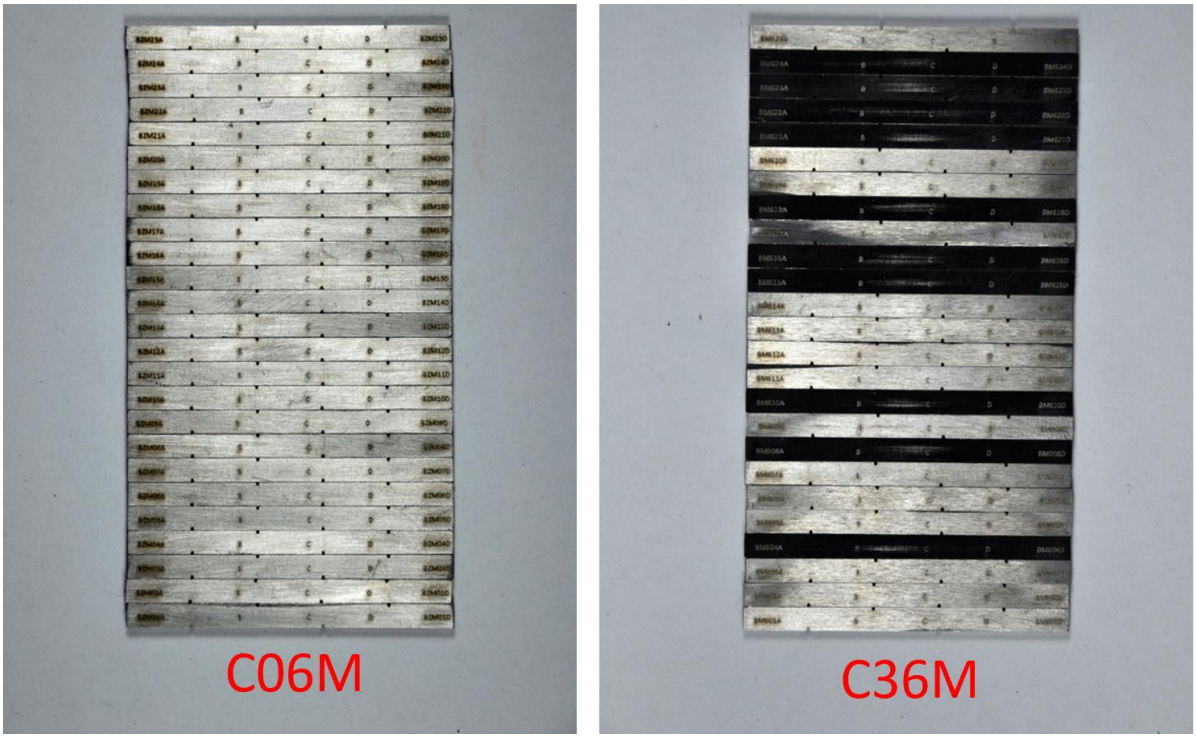

(b)

Figure 1. M4CVN specimen design (unit: mm) in (a) and actual machined specimens in (b) [6]

2.2 IRRADIATION CONDITIONS

The irradiation capsule design for the miniature four-notch Charpy bend bar specimens is illustrated below in Figure 2 and Figure 3. Specimens were arranged such that individual SiC thermometry specimens were paired directly with each C06M or C36M specimen, and the specimens were centered within an inner housing using a spring-loaded design. Variation of the gap (filled with inert gas) size between the inner housing and the outer capsule allowed for identical FCAB capsules to reach different irradiation temperatures during irradiation in HFIR. All FCAB capsules were irradiated in the flux trap positions of HFIR, and equivalent doses were computed using the accumulated neutron fluence at each specimen location and the FeCrAl composition for each capsule. The resulting doses achieved in dpa for each FCAB capsule are given in Table 2. The irradiation temperature was measured by SiC thermometry specimens using a dilatometer. To determine if there were any significant irradiation temperature gradients existing under irradiation, the SiC specimens, which spanned the entire length of the irradiation capsule, were sectioned into three equal segments and then tested. For each capsule, one SiC specimen with all three segments was tested with an additional middle segment from one of the other SiC specimens tested as well. Irradiation temperatures were determined using the algorithm and methods described by Campbell et al. [8]. The resulting mean irradiation temperature is summarized in Table 2. Different amounts of irradiation temperature gradients for all three capsules were observed. The mean irradiation temperatures were within a reasonable range from the target irradiation temperatures except for the FCAB06 capsule where the mean irradiation temperature was approximately 40°C lower than the target irradiation temperature but still above the expected range where the alloys of interest would phase segregate into α-α′ [9].

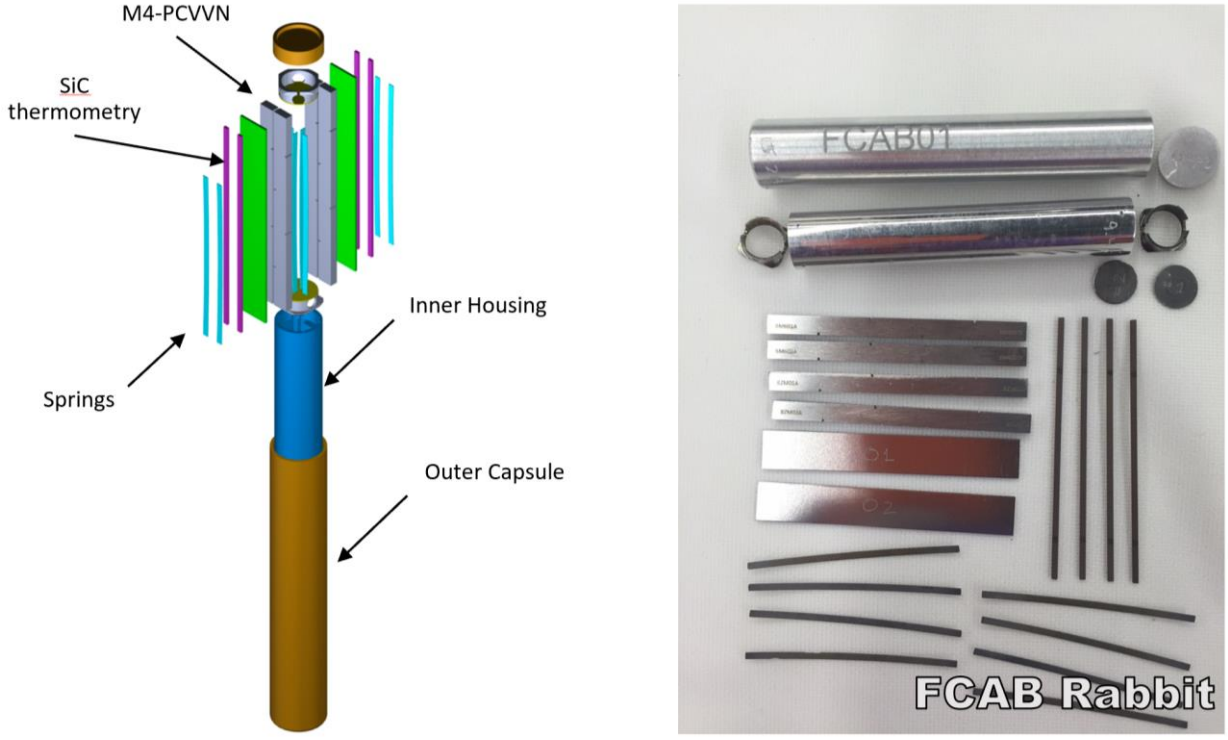

Figure 2. FCAB rabbit irradiation capsule design

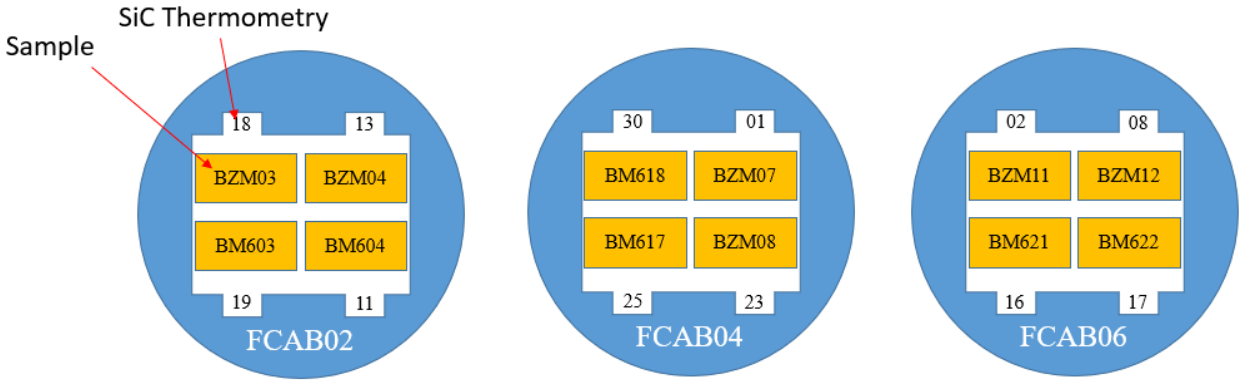

Figure 3. Arrangement of M4CVN bend bar and SiC thermometry specimens in FCAB capsules

Table 2. Summary irradiation conditions for FCAB02, FCAB04, and FCAB06 capsules

Capsule	Alloys	Specimen ID	Dose (dpa)	Target irradiation temperature (°C)	Maximum irradiation temperature gradient (°C)	Average irradiation temperature (°C)
FCAB02	C06M	BZM03 BZM04	17.6	200	45	204
	C36M	BM603 BM604				
FCAB04	C06M	BZM07 BZM08	18.3	330	23	343
	C36M	BM617 BM618				
FCAB06	C06M	BZM11 BZM12	18.6	550	57	507
	C36M	BM621 BM622				

2.3 TESTING TECHNIQUE AND EQUIPMENT

2.3.1 Vickers Microhardness

Post-irradiation Vickers microhardness testing was performed using a Mitutoyo HV-120 hardness tester in the hot cellas shown in Figure 4. The test procedure was based on the ASTM E384 standard [10] with 1 kg force and 15 sec dwell time. No sample preparation, e.g. polishing or grinding, was made before testing. As shown in Figure 5, four hardness measurements were made for each notch near the middle plane surrounding the end of the initial fatigue precrack. These hardness measurements were carefully chosen as to not affect the crack propagation path during the fracture toughness testing. This practice ensured a statistical measurement of the hardness near the crack initiation site during the following fracture toughness testing. Due to the partially recrystallized nature of the C06M and C36M specimens stemming from the choice of thermomechanical processing parameters used for their original fabrication and a small amount of irradiation temperature gradient along the length of the bend bar, it was of vital importance to get microhardness values in regions of the M4CVN bend bar specimens that were representative of the microstructure and irradiation temperature near the crack initiation site.

Figure 4. Vickers hardness tester in the hot cell facility

Figure 5. Vickers microhardness indentation pattern for M4CVN bend bar specimens. Dash lines indicate fatigue precrack prior to irradiation.

2.3.2 Master Curve Transition Fracture Toughness

Fracture toughness testing was performed using servo-hydraulic frames. The test frame used for the unirradiated specimens had 222.4 kN load capacity and the load cell had a calibrated 4.45 kN capacity. The testing temperature was measured directly from a thermocouple spot welded near each specimen notch. For irradiated specimens, testing was performed in the hot cell facility with a 444.8 kN load capacity servo-hydraulic frame with a calibrated load cell rated for 22.25 kN. Test temperature was measured from thermocouples spot welded to the end of the indenter tip which was in direct contact with the bend bar specimens in testing (Figure 6) and had been calibrated with a calibration specimen with a spot-welded thermocouple for the entire testing temperature range. For elevated temperature testing, a heat tape was used. Due to the upper operating temperature limit of the deflection gauge, the highest testing temperature was kept below 230°C.

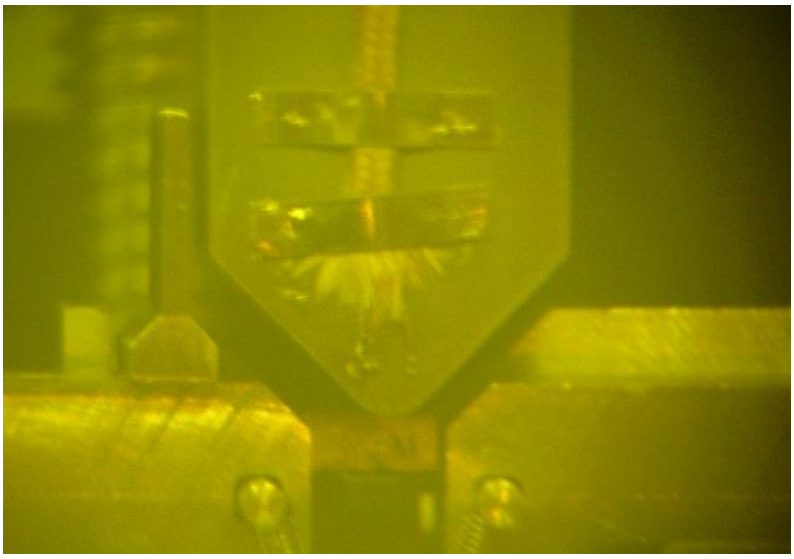

Figure 6. Thermocouples spot welded to the indenter tip in direct contact with the bend bar specimen

To test M4CVN bend bar specimens, we have designed a dedicated testing fixture shown in Figure 7. The deflection gauge attached to the specimen fixture was used to measure the load-line displacement of the specimen. The push bar can slide left and right and is used to push the specimen against the positioning block such that the specimen notch is aligned with the specimen indenter and the deflection gauge.

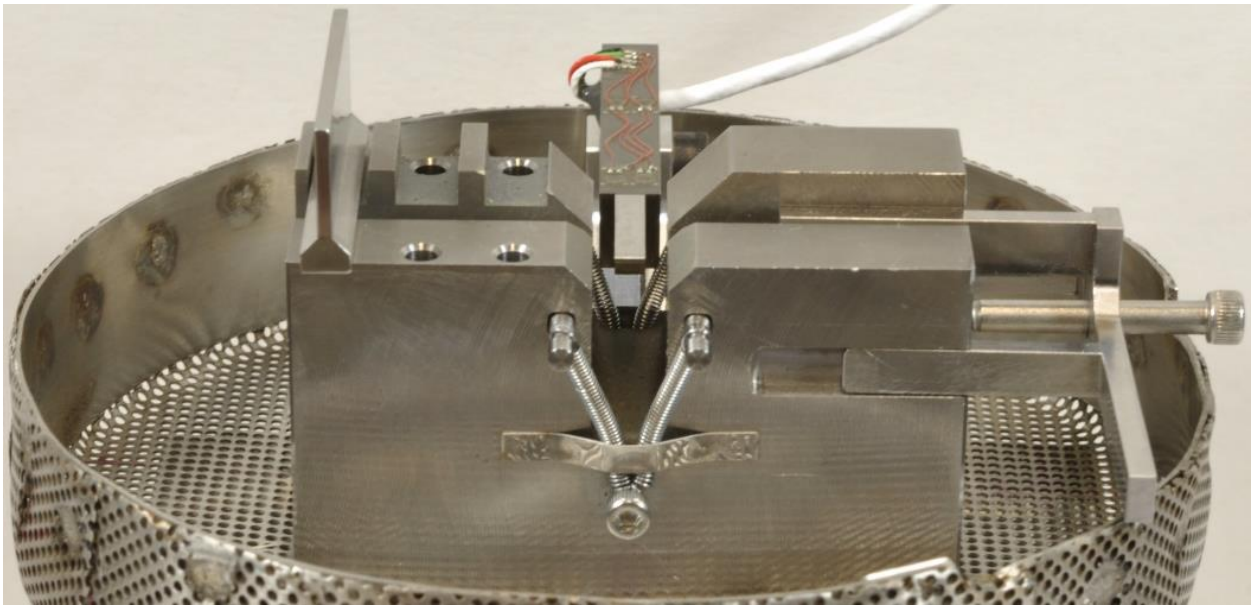

(a)

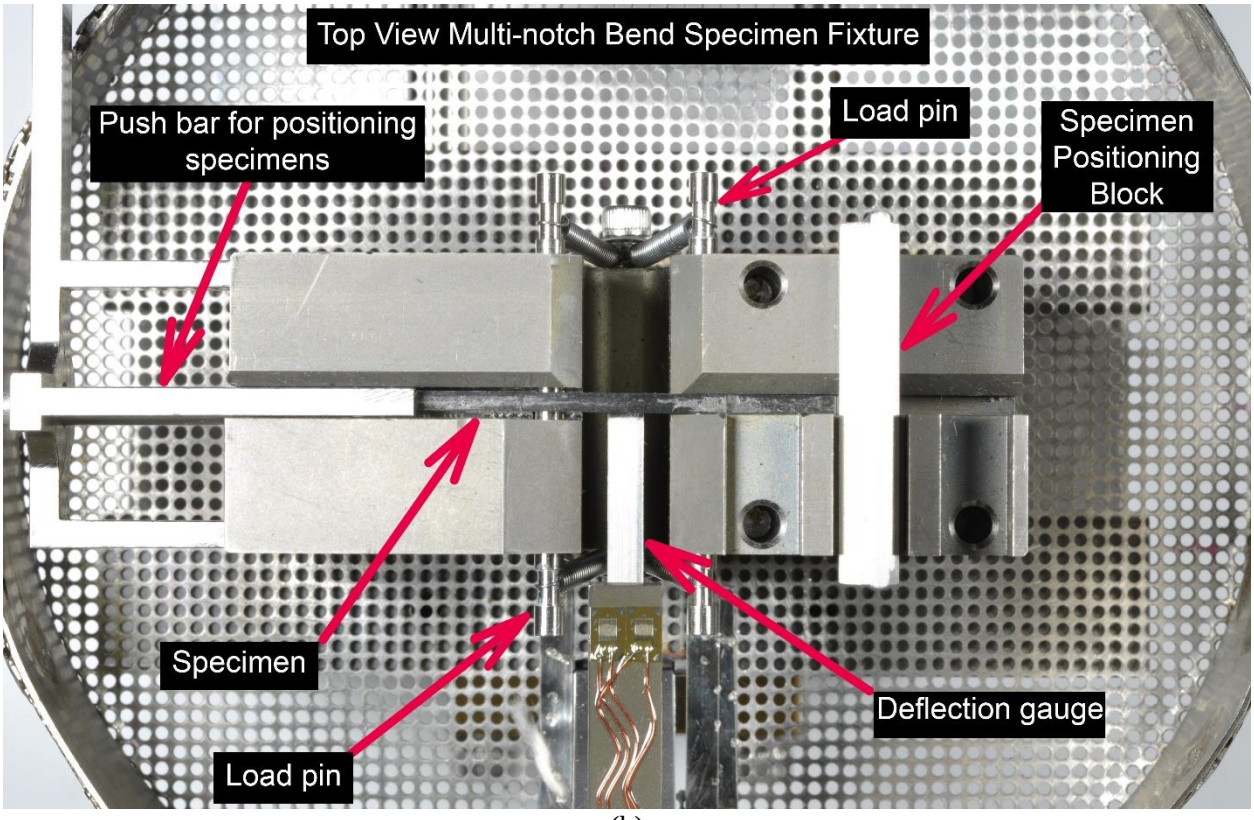

(b)

Figure 7. M4CVN bend bar specimen test fixture. (a) front view, (b) top view

We performed fracture toughness testing according to the ASTM E1921 Master Curve method. The test temperatures were selected by balancing between obtaining as high fracture toughness results as possible and still within the fracture toughness capacity limit $K_{Jclimit}$ given in Eq. (1):

$$K_{Jc\lim it} = \sqrt{\frac{Eb_o\sigma_{YS}}{30(1-\nu^2)}} \tag{1}$$

where:
E = material Young's modulus at the test temperature,
b_0 = length for the initial uncracked ligament,
σ_{YS} = material yield strength at the test temperature,
ν = Poisson's ratio.

Each specimen notch was tested until cleavage and then the crack length was measured from the fracture surface. The elastic-plastic equivalent stress intensity factor, K_{Jc}, was derived from the J-integral at the onset of cleavage fracture and size-adjusted to 1T (one-inch thickness) value based on the statistical weakest-link theory:

$$K_{Jc(1T)} = 20 + [K_{JC(o)} - 20](\frac{B_0}{B_{1T}})^{1/4} \tag{2}$$

where:
$K_{Jc(1T)} = K_{Jc}$ for a specimen thickness of one inch (B_{1T}=25.4 mm),
$K_{Jc(o)} = K_{Jc}$ for a specimen thickness of B_o (B_o=1.65 mm for M4CVN specimens).

We then calculated the Master Curve provisional reference temperature T_{oq} using a multi-temperature analysis method in Eq. (3) and K_{Jc} data were censored against both the fracture toughness capacity limit $K_{Jclimit}$ and the slow stable crack growth limit $K_{Jc\Delta a}$.

$$\sum_{i=1}^{N} \delta_i \frac{\exp[0.019(T_i - T_{oq})]}{11.0 + 76.7\exp[0.019(T_i - T_{oq})]} - \sum_{i=1}^{N} \frac{(K_{Jc(i)} - 20)^4 \exp[0.019(T_i - T_{oq})]}{\{11.0 + 76.7\exp[0.019(T_i - T_{oq})]\}^5} = 0 \tag{3}$$

where:
N = number of specimens tested,
T_i = test temperature corresponding to $K_{Jc(i)}$,
$K_{Jc(i)}$ = either a valid K_{Jc} datum or a datum replaced with a censoring value,
δ_i = 1.0 if the datum is valid or zero if the datum is a censored value,
T_{oq} = Master Curve provisional reference temperature solved by iterations.

3. RESULTS AND DISCUSSION

3.1 VICKERS MICROHARDNESS

The Vickers microhardness values for C06M and C36M are summarized below in Figure 8. Results for the unirradiated condition and 8 dpa capsules are added for comparison. In the unirradiated state, the microhardness variation between these two model FeCrAl alloys was small. However, due to differences in the fabrication history of C06M and C36M, it is difficult to attribute this small difference in initial hardness to singular changes in the Cr concentration. At the irradiation temperature of 501-507°C, both alloys showed a similar response to the high temperature irradiation, i.e., a small amount of irradiation softening with increasing irradiation doses. At 501-507°C, no Cr-rich α′ precipitates are expected based on the Fe-Cr and Fe-Cr-Al phase diagrams; furthermore, this irradiation temperature is above that required for dislocation loops to form [9,11-12]. Thus, the similar unirradiated microstructures, coupled with similar alloy compositions, helps explain the close irradiation responses of these alloys at this temperature. Moreover, at the irradiation temperature of 315-343°C, both alloys showed a similarly small amount of irradiation hardening which seemed to saturate for irradiation dose beyond 8 dpa. Although the microstructures of these specimens have not yet been quantified, it is expected that similar dislocation loop densities will exist [9]. At the lowest irradiation temperature of 166-204°C, both alloys showed significant irradiation hardening compared with high irradiation temperature cases, which is expected due to high densities of refined dislocation loops as seen in analogous samples irradiated to similar temperatures but at lower dose [9]. Similar to the irradiation at 315-343°C, the irradiation hardening at 166-204°C appeared to saturate for irradiation dose beyond 7 dpa.

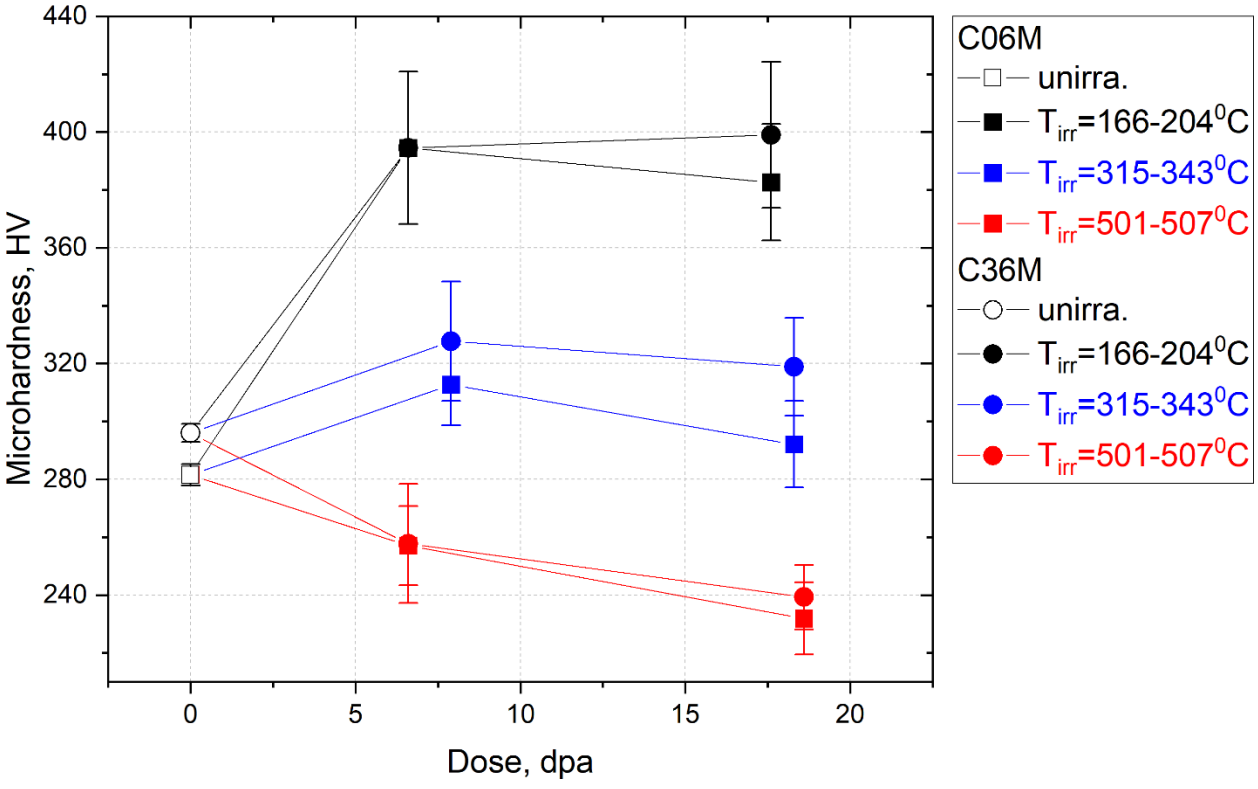

Figure 8. Vickers microhardness results before and after neutron irradiation for C06M and C36M. Error bars correspond to +/- one standard deviation

3.2 TRANSITION FRACTURE TOUGHNESS

The fracture toughness results of C06M and C36M after ~18 dpa irradiation are shown in Figure 9 and Figure 10, respectively. From Eq. (3), we calculated the Master Curve provisional reference temperature, T_{oq}, and then we plotted the Master Curve in Figures 9 and 10 using the following equation:

$$K_{Jc(med)} = 30 + 70\exp[0.019(T - T_{oq})] \quad (6)$$

where:
$K_{Jc(med)}$ = median fracture toughness for a multi-temperature data set from 1T size specimen,
T = test temperature,
T_{oq} = Master Curve provisional reference temperature.

Also shown in the same figures are fracture toughness capacity limit $K_{Jclimit}$ calculated from Eq. (1) and the tolerance bounds calculated using the equation below:

$$K_{Jc(0.xx)} = 20 + [\ln(\frac{1}{1-0.xx})]^{1/4}\{11 + 77\exp[0.019(T - T_{oq})]\} \quad (7)$$

where:
0.xx = selected cumulative probability level, e.g., for the 2% tolerance bound, 0.xx=0.02.

Due to the small size of M4CVN specimens, the fracture toughness capacity limit $K_{Jclimit}$ of the specimen was very low, which mandated testing in the temperature region more than 50°C lower than the derived provisional Master Curve reference temperature (T_{0q}) to avoid exceeding $K_{Jclimit}$. Based on the current ASTM E1921 standard, this violated the minimum testing temperature requirement and therefore the provisional value cannot be qualified as Master Curve reference temperature, T_0. Nonetheless, most valid fracture toughness data (data points below the blue dashed line for $K_{Jclimit}$) in Figures 9 and 10 are bounded by the 2% and 98% tolerance boundaries of the Master Curve. In addition, our past study shows that the Master Curve reference temperature determined by the miniature bend bar specimens is essentially the same as that determined by conventional larger size specimens [6, 13-16].

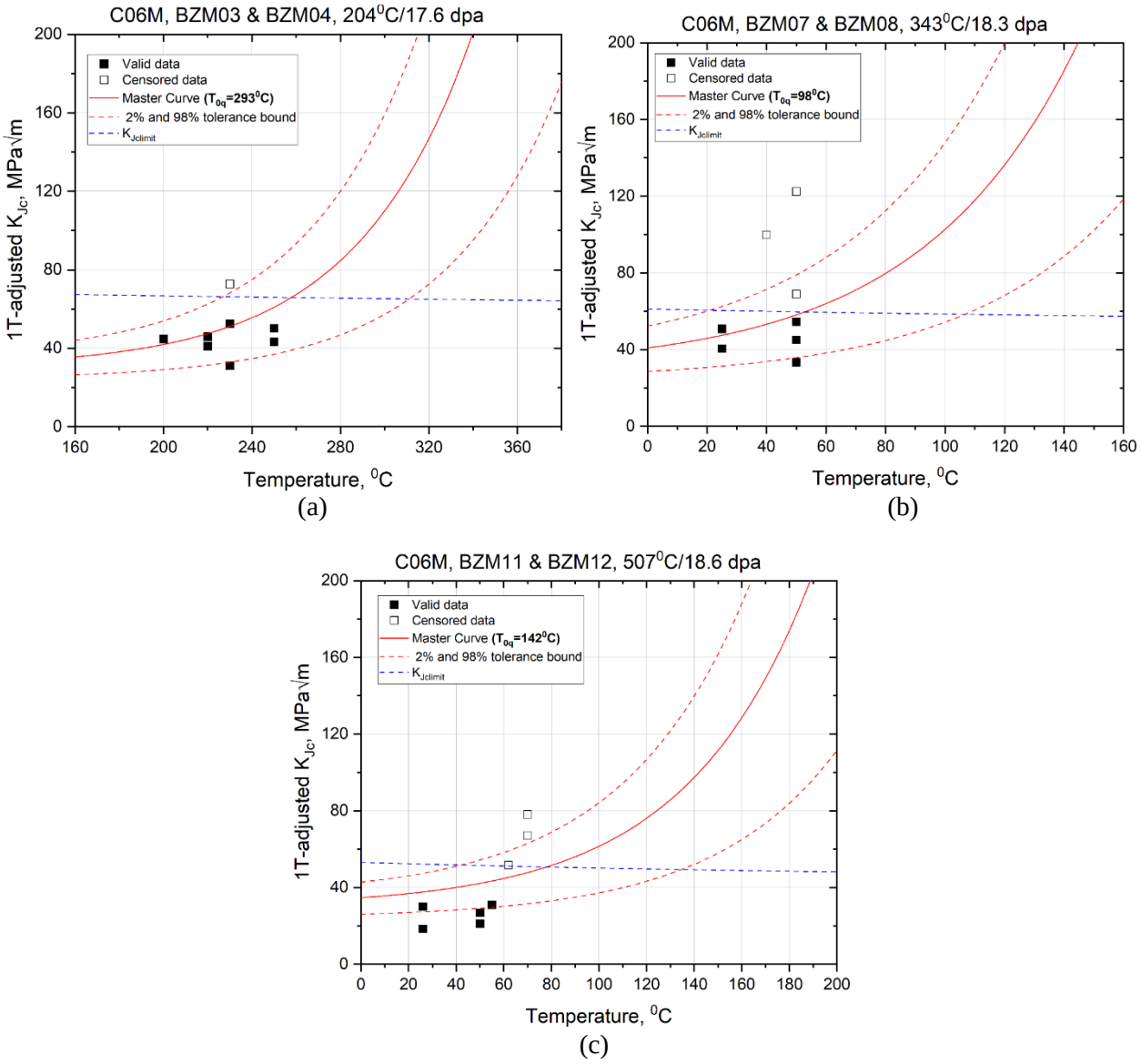

Figure 9. Master Curve fracture toughness results for C06M. (a) 204°C/17.6dpa, (b) 343°C/18.3dpa, (c) 507°C/18.6dpa

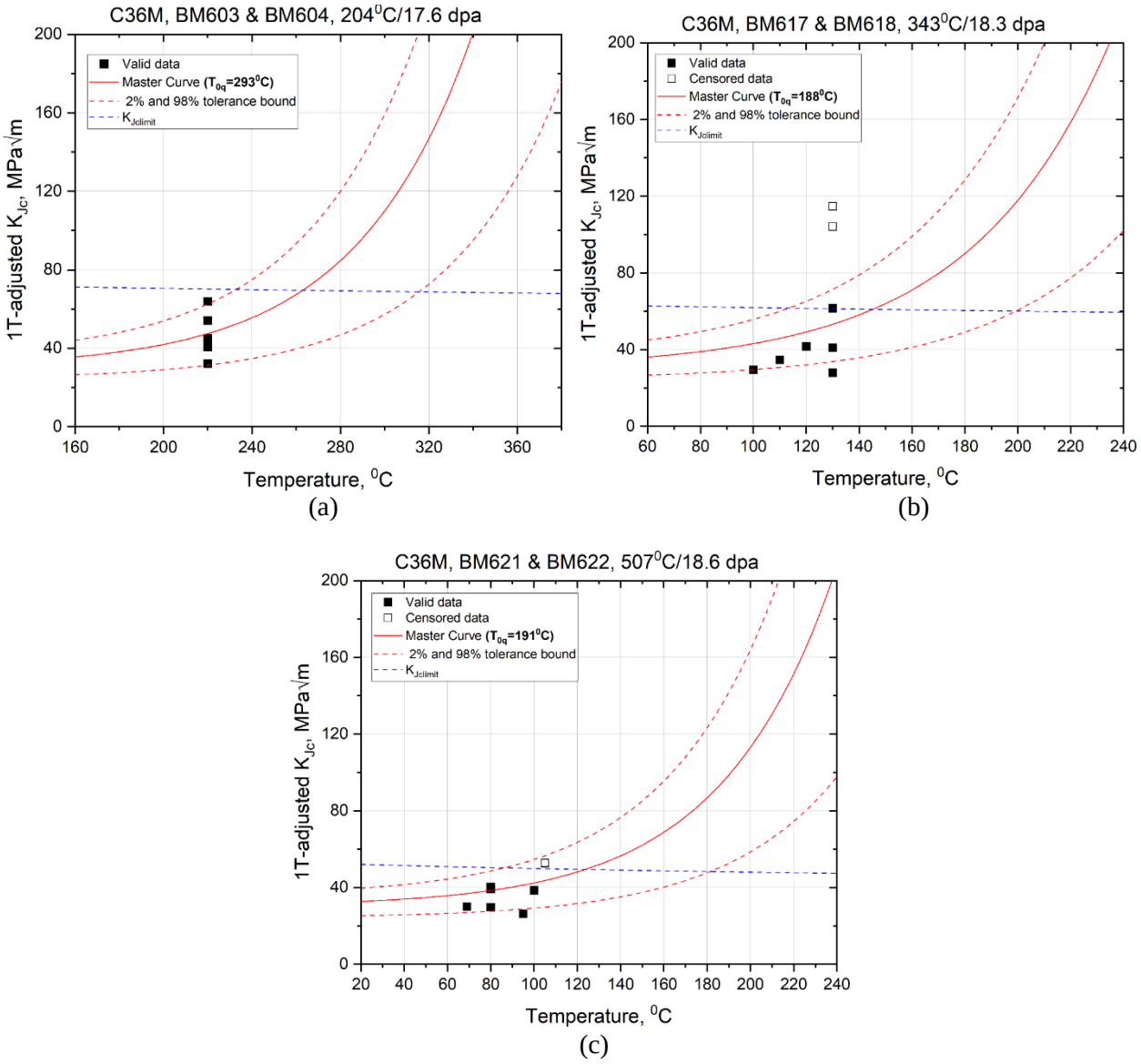

Figure 10. Master Curve fracture toughness results for C36M. (a) 204°C/17.6dpa, (b) 343°C/18.3dpa, (c) 507°C/18.6dpa

Post-test fracture surface image indicated brittle fracture as the failure mechanism for the ~18 dpa M4CVN specimens. One example of such fracture surface is shown in Figure 11.

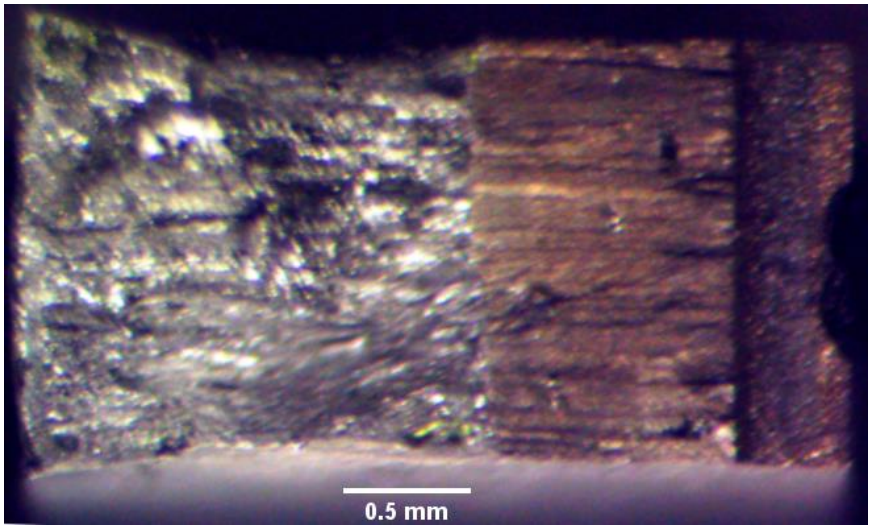

Figure 11. Post-test fracture surface image of one failed ~18 dpa M4CVN specimen after 507°C/18.6dpa irradiation.

As shown in Figure 12, for both C06M and C36M, the irradiation temperature played a distinctly different role in irradiation embrittlement. For irradiation at two higher temperature ranges, i.e., 315-343°C and 501-507°C, post-irradiation evaluation discovered similar T_{0q} as the unirradiated condition for both materials, meaning no additional irradiation induced embrittlement at these irradiation conditions. In contrast, when irradiated at the low temperature range, i.e., 166-204°C, significant irradiation embrittlement demonstrated by a sharp increase in T_{0q} was observed in both materials. Moreover, no significant differences were observed in T_{0q} between the 7 dpa irradiation and ~18 dpa irradiation, indicating the irradiation effect on T_{0q} likely saturated beyond 7 dpa. C06M showed a lower T_{0q}, meaning better toughness, than C36M at the unirradiated condition, and such trend was kept even after neutron irradiation except for the 166-204°C irradiation where both materials had similar T_{0q}.

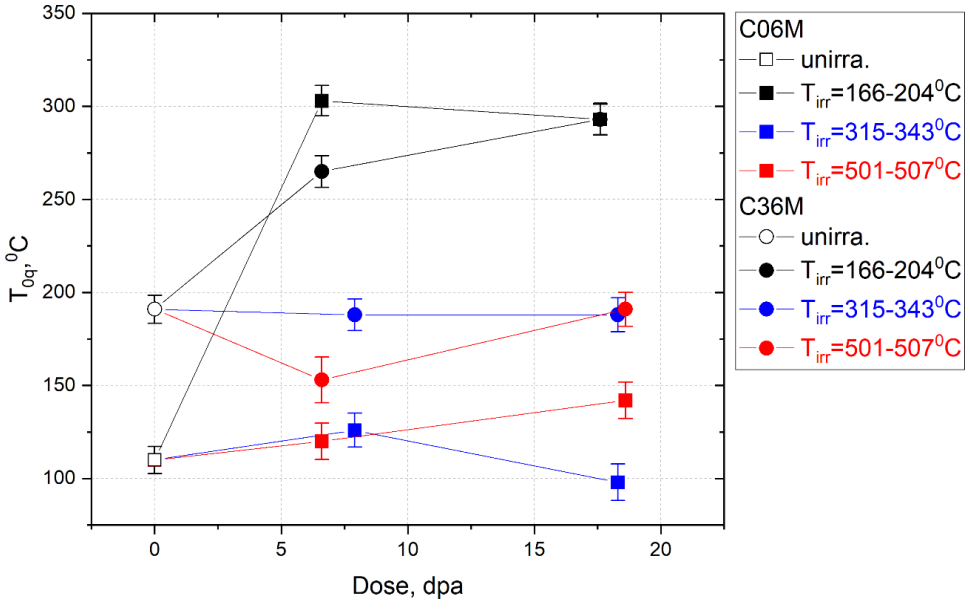

Figure 12. Master Curve reference temperature T_{0q} before and after neutron irradiation for C06M and C36M. Error bars correspond to +/- one standard deviation.

Figure 13 compares the correlation between irradiation hardening and irradiation embrittlement for both materials. No obvious linear correlation between the microhardness and T_{0q} was observed in either material. For the unirradiated condition and irradiation at 315-343°C and 501-507°C, despite the change in microhardness, there was no apparent change in T_{0q}. In contrast, the low temperature irradiation at 166-204°C resulted in significant irradiation hardening and embrittlement compared with the unirradiated condition.

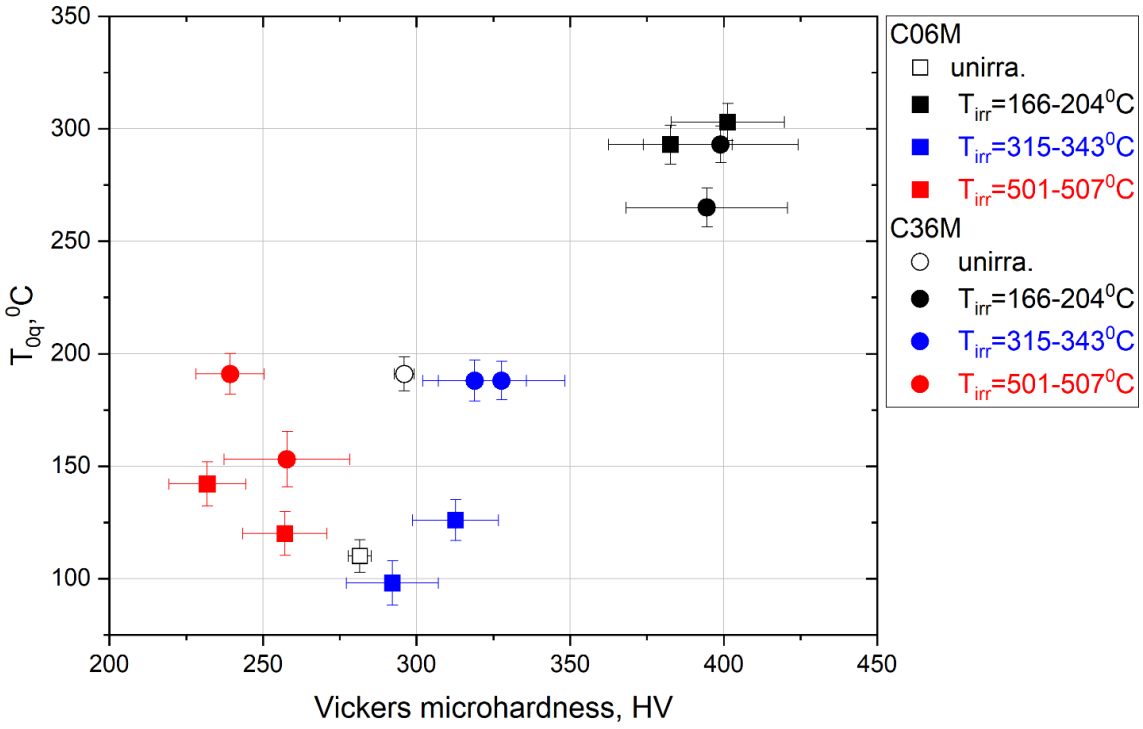

Figure 13. Correlation between microhardness and Master Curve transition temperature T_{0q} for C06M and C36M. Error bars correspond to +/- one standard deviation

4. CONCLUSIONS

FeCrAl alloys are promising candidate materials for the ATF cladding applications due to their excellent corrosion resistance to the elevated temperature steam environment. However, the fracture toughness of FeCrAl alloys may be a critical factor and needs to be evaluated in its deployment for nuclear power applications. In this study, we performed post-irradiation microhardness and Master Curve fracture toughness characterization on two Generation II FeCrAl alloys, i.e., C06M and C36M. The measured irradiation conditions were: 204°C/17.6dpa, 343°C/18.3dpa, and 507°C/18.6dpa. The main conclusions of this study can be summarized as followings:

1) After the 204°C/17.6dpa irraidiation, both materials exhibited significant irradiation hardening and embrittlement
2) After the 343°C/18.3dpa irraidiation, both materials exhibited small irradiation hardening without irradiation embrittlement
3) After the 507°C/18.6dpa irraidation, both materials exhibited irradiation softening without irradiation embrittlement

4) Comparing the microhardness and Master Curve reference temperature T_{0q} before and after neutron irradiation, we did not observe any linear correlation between the two parameters for both materials mainly due to a flat response of the Master Curve reference temperature T_{0q} to the irradiations at 166-204°C and 315-343°C ranges
5) C06M showed a lower T_{0q}, meaning better toughness, than C36M at the unirradiated condition and such trend was kept even after neutron irradiation except for the 166-204°C irradiation where both materials had similar T_{0q}.
6) In terms of hardening and embrittlement, the irradiation effect on both materials appeared to be saturated after an irradiation dose of 7 dpa.

5. REFERENCES

1. K.G. Field, M.A. Snead, Y. Yamamoto, B.A. Pint, K.A. Terrani, Materials properties of FeCrAl alloys for nuclear power production applications, ORNL/TM-2017/186. (2017). doi:10.2172/1400207.

2. Z. Sun, Y. Yamamoto, X. Chen, Impact toughness of commercial and model FeCrAl alloys, Mater. Sci. Eng. A. (2018). doi:10.1016/J.MSEA.2018.07.074.

3. W. Chubb, S. Alfant, A.A. Bauer, E.J. Jablonowski, F.R. Shober, R.F. Dickerson, Constitution, metallurgy, and oxidation resistance of iron-chromium-aluminum alloys: BMI-1298, (1958).

4. K.G. Field, Y. Yamamoto, R.H. Howard, Status of Post Irradiation Examination of FCAB and FCAT Irradiation Capsules, ORNL/TM-2016/558. (2016).

5. X. Chen, K.G. Field, D. Zhang, C. Massey, J.P. Robertson, K. Linton, A. Nelson, Post-Irradiation Fracture Toughness Characterization of Generation II FeCrAl Alloys, ORNL/TM-2019/1391, October 2019.

6. X. Chen, M.A. Sokolov, L.N. Clowers, Y. Katoh, M. Rieth, Master Curve fracture toughness characterization of Eurofer97 steel variants using miniature multi-notch bend bar specimens for fusion applications, Proceedings of the ASME 2018 Pressure Vessels and Piping Conference, PVP2018-85065, July 15-20, 2018, Prague, Czech Republic.

7. ASTM E1921-17a: Standard Test Method for Determination of Reference Temperature, T0, for Ferritic Steels in the Transition Range, ASTM International, West Conshohocken, PA, 2017.

8. A.A. Campbell, W.D. Porter, Y. Katoh, L.L. Snead, Method for analyzing passive silicon carbide thermometry with a continuous dilatometer to determine irradiation temperature, Nucl. Instruments Methods Phys. Res. Sect. B Beam Interact. with Mater. Atoms. 370 (2016) 49–58. doi:10.1016/j.nimb.2016.01.005.

9. C.P. Massey, D. Zhang, S.A. Briggs, P.D. Edmondson, Y. Yamamoto, M.N. Gussev, K.G. Field, Deconvoluting the Effect of Chromium and Aluminum on the Radiation Response of Wrought FeCrAl Alloys After Low-Dose Neutron Irradiation, Journal of Nuclear Materials 549 (2021): 152804.

10. ASTM E384-17, Standard Test Method for Microindentation Hardness of Materials, ASTM International, West Conshohocken, PA, 2017.

11. K.G. Field, S.A. Briggs, Radiation Effects in FeCrAl Alloys for Nuclear Power Applications, Comprehensive Nuclear Materials (Second Edition), Editors: R.J.M. Konings, R.E. Stoller, (2020): 293-306, doi: 10.1016/B978-0-12-803581-8.11613-3.

12. K.G. Field, K.C. Littrell, S.A. Briggs, Precipitation of α′ in neutron irradiated commercial FeCrAl alloys, Scripta Materialia 142 (2018): 41-45.

13. X. Chen, M.A. Sokolov, A. Bhattacharya, L.N. Clowers, T. Graening, Y. Katoh, M. Rieth, Master Curve Fracture Toughness Characterization of Eurofer97 Steel Variants Using Miniature Multi-notch

Bend Bar Specimens for Fusion Applications, Proceedings of the ASME 2019 Pressure Vessels and Piping Conference, PVP2019-93797, July 14-19, 2019, San Antonio, TX, USA.

14. M. Sokolov, H. Tanigawa, Fusion Reactor Materials Program Semiannual Progress Report, DOE/ER-0313/41, December 31, 2006, p83.

15. M. Sokolov, H. Tanigawa, Fusion Reactor Materials Program Semiannual Progress Report, DOE/ER-0313/33, December 31, 2002, p105.

16. X. Chen, M.A. Sokolov, K.D. Linton, L.N. Clowers, Y. Katoh, Transition fracture toughness characterization of Eurofer97 steel using pre-cracked miniature multi-notch bend bar specimens, ORNL/LTR-2017/532, November 30, 2017.